AFRL-RX-WP-JA-2016-0321

ANALYSIS OF NON-CONTACT ACOUSTO-THERMAL SIGNATURE DATA (POSTPRINT)

Amanda K. Criner

AFRL/RX

Norman Schehl

University of Dayton Research Institute

16 October 2015
Interim Report

Distribution Statement A.
Approved for public release: distribution unlimited.

(STINFO COPY)

AIR FORCE RESEARCH LABORATORY
MATERIALS AND MANUFACTURING DIRECTORATE
WRIGHT-PATTERSON AIR FORCE BASE, OH 45433-7750
AIR FORCE MATERIEL COMMAND
UNITED STATES AIR FORCE

REPORT DOCUMENTATION PAGE

Form Approved
OMB No. 0704-0188

1. REPORT DATE *(DD-MM-YY)*
16 October 2015

2. REPORT TYPE
Interim

3. DATES COVERED *(From - To)*
31 October 2014 – 16 September 2015

4. TITLE AND SUBTITLE
ANALYSIS OF NON-CONTACT ACOUSTO-THERMAL SIGNATURE DATA (POSTPRINT)

5a. CONTRACT NUMBER
FA8650-14-D-5224-0003

5b. GRANT NUMBER

5c. PROGRAM ELEMENT NUMBER
61102F

6. AUTHOR(S)
1) Amanda K. Criner – AFRL/RX
2) Norman Schehl – UDRI

5d. PROJECT NUMBER
3003

5e. TASK NUMBER 0003

5f. WORK UNIT NUMBER
X0Y6

7. PERFORMING ORGANIZATION NAME(S) AND ADDRESS(ES)
1) AFRL/RX
Wright-Patterson Air Force Base
OH, 45433

2) University of Dayton Research Institute, Structural Integrity Division, 300 College Park, Dayton, OH 45469-0120

8. PERFORMING ORGANIZATION REPORT NUMBER

9. SPONSORING/MONITORING AGENCY NAME(S) AND ADDRESS(ES)
Air Force Research Laboratory
Materials and Manufacturing Directorate
Wright-Patterson Air Force Base, OH 45433-7750
Air Force Materiel Command
United States Air Force

10. SPONSORING/MONITORING AGENCY ACRONYM(S)
AFRL/RXCA

11. SPONSORING/MONITORING AGENCY REPORT NUMBER(S)
AFRL-RX-WP-JA-2016-0321

12. DISTRIBUTION/AVAILABILITY STATEMENT
Distribution Statement A. Approved for public release: distribution unlimited.

13. SUPPLEMENTARY NOTES
PA Case Number: 88ABW-2015-4957; Clearance Date: 16 Oct 2015. This document contains color. Journal article published in AIP Conference Proceeding, Vol. 1706, No. 1, Feb 2016. © 2016 AIP Publishing. The U.S. Government is joint author of the work and has the right to use, modify, reproduce, release, perform, display, or disclose the work.
The final publication is available at doi: 10.1063/1.4940566

14. ABSTRACT *(Maximum 200 words)*
The non-contact acousto-thermal signature (NCATS) is a nondestructive evaluation technique with potential to detect fatigue in materials such as noisy titanium and polymer matrix composites. The determination of underlying physical mechanisms and properties may be determined by parameter estimation via nonlinear regression. The nonlinear regression analysis formulation, including the underlying models, is discussed. Several models and associated data analyses are given along with the assumptions implicit in the underlying model. The results of these analyses are discussed.

15. SUBJECT TERMS
Non-contact acousto-thermal signature (NCATS); nondestructive evaluation technique; fatigue; titanium and polymer matrix composites

16. SECURITY CLASSIFICATION OF:			17. LIMITATION OF ABSTRACT:	18. NUMBER OF PAGES	19a. NAME OF RESPONSIBLE PERSON (Monitor)
a. REPORT	b. ABSTRACT	c. THIS PAGE			Amanda Criner
Unclassified	Unclassified	Unclassified	SAR	8	19b. TELEPHONE NUMBER *(Include Area Code)* (937) 255-9797

Analysis of Non-contact Acousto-Thermal Signature Data

Amanda K. Criner[1,a)] and Norman Schehl[2]

[1]*Air Force Research Laboratory, Materials and Manufacturing Directorate, Wright Patterson AFB, OH 45433-7817*
[2]*University of Dayton Research Institute, Structural Integrity Division, 300 College Park, Dayton, OH 45469-0120*

[a)]Corresponding author: amanda.criner.1@us.af.mil

Abstract. The non-contact acousto-thermal signature (NCATS) is a nondestructive evaluation technique with potential to detect fatigue in materials such as noisy titanium and polymer matrix composites. The determination of underlying physical mechanisms and properties may be determined by parameter estimation via nonlinear regression. The nonlinear regression analysis formulation, including the underlying models, is discussed. Several models and associated data analyses are given along with the assumptions implicit in the underlying model. The results of these analyses are discussed.

Background and Experimental Procedure

Non-Contact Acousto-Thermal Signature (NCATS) uses the conversion of acoustic energy to heat to characterize evolving damage in materials. When high amplitude acoustic waves encounter a material boundary they both reflect from and transmit into the material. The energy absorbed in the material is subsequently converted to heat through the diffusion of transverse thermal currents, inter-crystalline thermal currents, and dislocation motion [1, 2]. In these experiments, high amplitude acoustic waves propagated through an air gap and interacted with a Titanium sample. The experimental setup to quantify the thermal response consisted of an ultrasonic horn operating at 20 kHz, an IR camera, a flat specimen, and a servo hydraulic machine that is used to apply fatigue cycles to the specimen. The 20 kHz sonic horn was placed 480 μm from the specimen as shown in Figure 1(a) and was pulsed for 1000 ms. The sonic horn does not contact the specimen even at full amplitude. Temperature rise in a Titanium specimen, due to the conversion of sonic energy to heat, was measured by an Indigo-Merlin Infrared (IR) camera located 190 mm from the specimen also shown in Figures 1(a) and (b). This work evaluated experimental data from 2 trials at 80% sonic horn power and 3 trials at 100% power. A sophisticated analysis of one trial at 100% power, including curve fitting, is presented.

A custom developed system and software were used to control the sonic horn pulse and the acquisition of thermal response data from the IR camera. The firing of the sonic horn and the thermal response data collection were synchronized, with the start of the horn pulse equating to time zero. Thermal response data was collected at 15 frames per second for a total of 30 seconds, and data was simultaneously collected at multiple points in the IR camera field of view. Temperature data used in this analysis begins when the sonic horn pulse ceases at 1000 ms. The spatial resolution of the IR camera for this experimental configuration was determined to be 250 μm.

The Ti-6Al-4V specimens chosen for this study were flat rectangular bars having a width of 50.8 mm, a thickness of 3.2 mm, and a nominal length of 200 mm. The specimens used in this study contained a geometric feature, a 6.4 mm diameter open hole. The Ti-6Al-4V material has an equiaxed microstructure with an average grain size of 20 μm. To increase the emissivity, the specimen was painted black in the region of interest on the side of the specimen facing the IR camera.

Data Analysis

The initial goal of the data analysis was to identify, detect or discern the physical methods occurring in the NCATS experiment. This task requires sophisticated data analysis techniques including hypothesis testing and information theoretic based model selection (such as the Akaike Information Criterion–AIC). Both hypothesis testing

42nd Annual Review of Progress in Quantitative Nondestructive Evaluation
AIP Conf. Proc. 1706, 100006-1–100006-6; doi: 10.1063/1.4940566

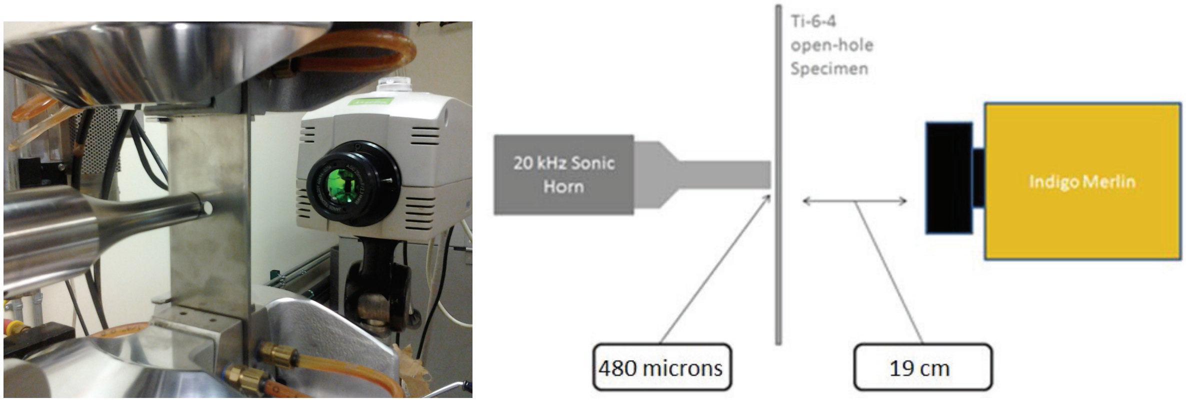

(a) (b)

FIGURE 1. (a) NCATS experimental setup with sonic horn, specimen, and IR camera (b) Sonic Horn and IR camera spacing relative to the specimen

(see [3, 4] for examples) and the AIC (an example is given in [5] and a thorough introduction may be found in [6]) require that parameter estimation be carried out. In order to carry out parameter estimation, a model (which depends on quantities of interest and the independent variables) and data are needed. The data must include the measurement of the signal and the value of the independent variable at that measurement. Initial data analyses were carried out using single location data (with dependent variable time), and a 1D thermal model. These produced anomalous results. Thermal models which capture the 3D geometry of the specimens were considered. In order to analyze the ensemble data of the 36 cursor locations on the back surface over all the times, all the independent variables must be known. The independent variables for this experiment are time and spatial coordinates. For some of the data sets, the value of the spatial coordinates were not known. Data that was collected previously [2] were used instead. The videos were used to compare with the specimen to determine the location of the pixels relative to each other. The pixels were found to be 0.25 mm by 0.25 mm which confirmed the measurements from previous work.

In the classic paper by Parker *et al.* [7], the authors derive a flash method to determine several thermal properties of materials, including the thermal diffusivity. The derivation of this method is discussed below. Throughout the discussion the method and estimate are referred to as the "Parker method" and "Parker estimate," respectively. The Parker estimate of the thermal diffusivity $\hat{\alpha}_P$ is obtained by making several assumptions about the sample. Using these assumptions, a series solution may be derived and then truncated to obtain the Parker result. The assumptions implicit in using this method are equivalent to assuming the temperature u is the solution to the heat equation which is given by the partial differential equation

$$u_t - \alpha u_{zz} = 0 \quad \text{for} \quad 0 < z < L. \tag{1}$$

The thermal diffusivity is given by α mm^{2}s^{-1} and the length that the heat passes through is given by L mm. Parker's method further assumes no loss on the boundaries (perfectly insulated boundaries) which corresponds to Neumann boundary conditions

$$\begin{aligned} -\alpha u_z|_{z=0} &= 0 \\ \alpha u_z|_{z=L} &= 0. \end{aligned} \tag{2}$$

In Parker's method for flash heating, rather than representing the flash by a source on the boundary, the flash is assumed to be uniformly absorbed in a small region near the heated boundary (the $z = 0$ boundary here) yielding the Heaviside initial temperature

$$u(0, z) = \begin{cases} T_L = \frac{Q}{\rho c_p g} & \text{for } 0 < z < g \\ 0 & \text{for } g < z < L \end{cases} \tag{3}$$

where Q (J cm^{-2}) is the radiant energy of the flash, g (mm) is the depth that it is uniformly absorbed, ρ (g mm^{-3}) is the density and c_p (J kg^{-1}K^{-1}) is the heat capacity. A well established result from Parker is that given the temperature

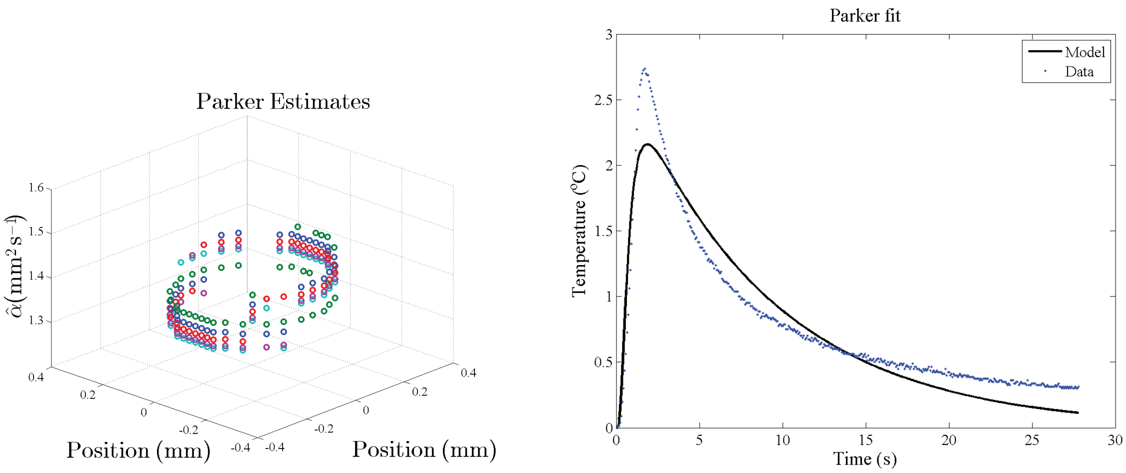

(a)

(b)

FIGURE 2. (a) Parker estimates of the thermal diffusivity at each location, for each trial. (b) An example fit.

corresponds to a solution of equations (1)–(3), the thermal diffusivity may be estimated as

$$\hat{\alpha}_P = 1.38L^2/\pi^2 t_{1/2}, \tag{4}$$

where $t_{1/2}$ is the time that the back surface reaches 1/2 of the maximum temperature. The estimates for each location on the sample are given in Figure 2(a). The handbook value for the thermal diffusivity of Ti-6Al-4V is 2.75 $\mathrm{mm^2s^{-1}}$ [8]. The Parker estimates obtained by applying Equation 4 to the data from each of the 36 locations from each of the five trials are depicted in Figure 2(a). It is clear in this figure that the Parker estimates are about half the handbook value. A further problem with the Parker estimates is that the implicit assumptions are clearly not valid. One clear violation of these assumptions is loss on the boundary. Cooling may be observed after two seconds in the data from one location during one trial (see Figure 2(b)). This model assumption can be relaxed by replacing the insulated boundary condition in Equation 3 with boundary conditions with losses

$$-\alpha u_z|_{z=0} = -\lambda_0 u(t, 0) \tag{5}$$
$$\alpha u_z|_{z=L} = -\lambda_L u(t, L) \tag{6}$$

where λ_0 and λ_L (mm $\mathrm{s^{-1}}$) are the losses on the right and left boundary respectively. This model was approximated numerically by the finite element method [9]. The left side temperature $T_L = \frac{Q}{\rho c_p g}$ and the absorption depth g in Parker initial condition in (3), the thermal diffusivity in the heat equation (1) and the loss terms in the boundary conditions (6) were estimated using nonlinear least squares. The estimated thermal diffusivity was 0.225 $\mathrm{mm^2s^{-1}}$ which is an order of magnitude less than the handbook value of 2.75 $\mathrm{mm^2s^{-1}}$. The resulting model values also do not fit that data well as can be seen in Figure 2(b).

The poor fit and lack of correspondence of the estimated thermal diffusivity with the handbook value indicate that there may be other invalid assumptions that are effecting the results. The thermal image of the specimen 12 ms after the horn is turned off in Figure 3(a) suggests that the heating is nonuniform. There does appear to be radial symmetry which leads us to consider a radially symmetric cylindrical domain. It is further assumed that the edges are far enough away to be considered infinite. The corresponding partial differential equation is given by

$$\begin{aligned} u_t - \alpha\left(\frac{(ru_r)_r}{r} + u_{zz}\right) &= 0 \\ u_r|_{r=0} &= 0 \\ \lim_{r\to\infty} u &= 0 \\ -\alpha u_z|_{z=0} &= -\lambda_0 u(t, r, 0) \end{aligned} \tag{7}$$

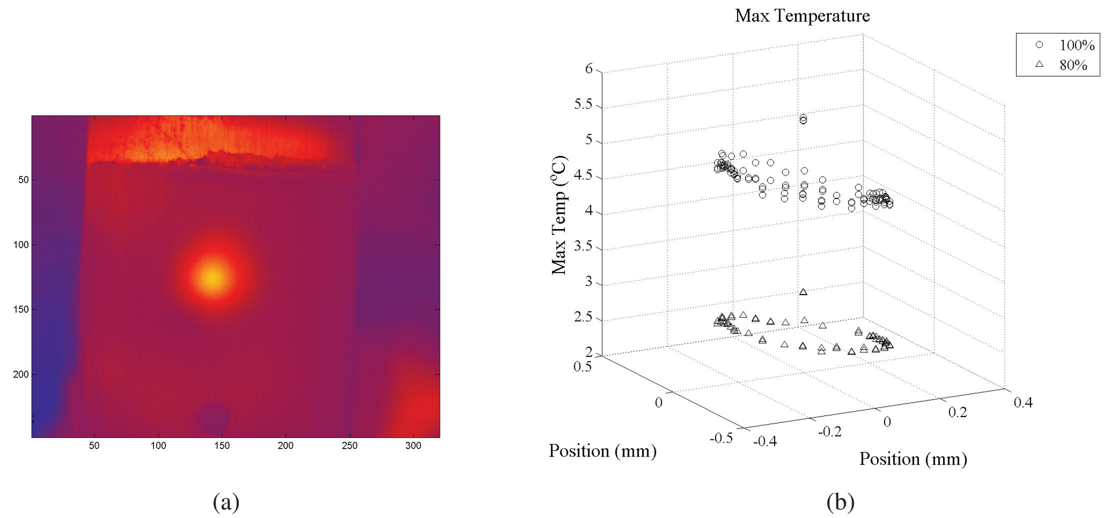

FIGURE 3. (a) An example thermal image from the experiment (b) The maximum temperature sensitivity to amplitude

$$\alpha u_z|_{z=L} = -\lambda_L u(t, r, L)$$
$$u(0, r, z) = u_0(r, z)$$

where r is the radius and z is the depth in the specimen (in mm). For the cylindrical parameter estimation, the losses on the boundaries were assumed to be equal, so $\lambda_0 = \lambda_L = \lambda$. The partial differential equation with boundary and initial conditions (7) was solved with finite differences and the finite volume method. The results presented here were computed using the finite volume method.

The logistic function is a smooth approximation of the Heaviside function. For instance, the Parker initial condition (3) may be smoothly approximated by

$$f(z) = \frac{T_L}{1 + e^{15(z-g)}}, \tag{8}$$

where the constant 15 was chosen arbitrarily. The radially symmetric, with discontinuity at $(r, z) = (r_0, z_0)$ rather than

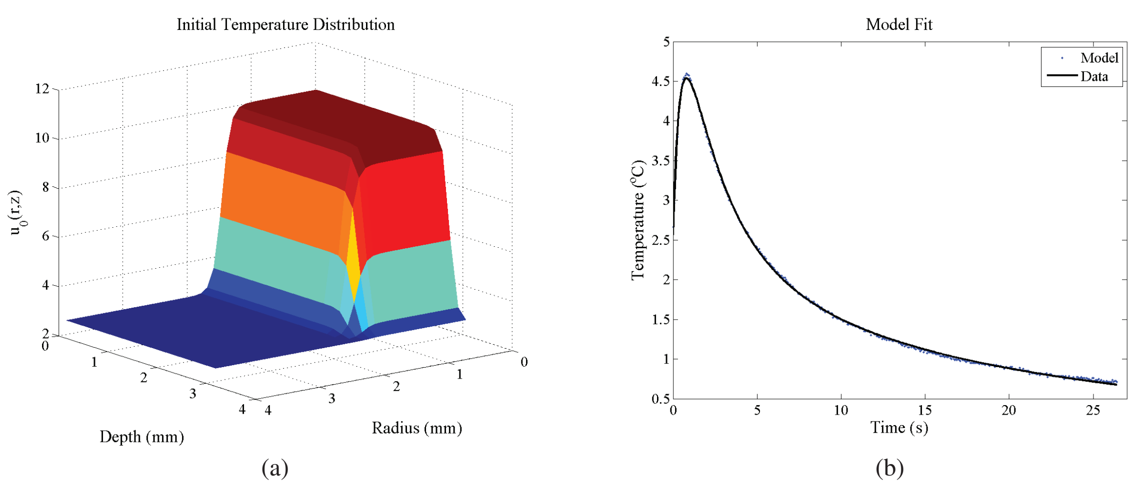

FIGURE 4. (a) Estimated initial temperature distribution using (9) (b) Estimated fit

$z = g$ as in (8), version of this is given by

$$u_0(r,z) = \frac{T_L}{\left(1 + e^{15(z-z_0)}\right)\left(1 + e^{15(r-r_0)}\right)} + T_R, \tag{9}$$

the right side temperature T_R is fixed to be the value of the observed temperature at $t = 1$s. This time value was chosen because it is when the horn was turned off. The subsequent data that is presented here begins at $t \geq 1$. The above initial condition gives a temperature profile that is approximately T_L for depths less than z_0 ($z < z_0$) and radii less than r_0 ($r < r_0$), and T_R everywhere else. Using this initial condition, the estimated thermal diffusivity (α) and loss were approximately 0.22. The estimated thermal diffusivity was is an order of magnitude less than the handbook value. The estimated initial condition (T_L, z_0, and r_0 were estimated) is given in Figure 4(a). The curve fit using this model and initial condition were much better than the fit using the 1D models. The curve fit is given in Figure 4(b).

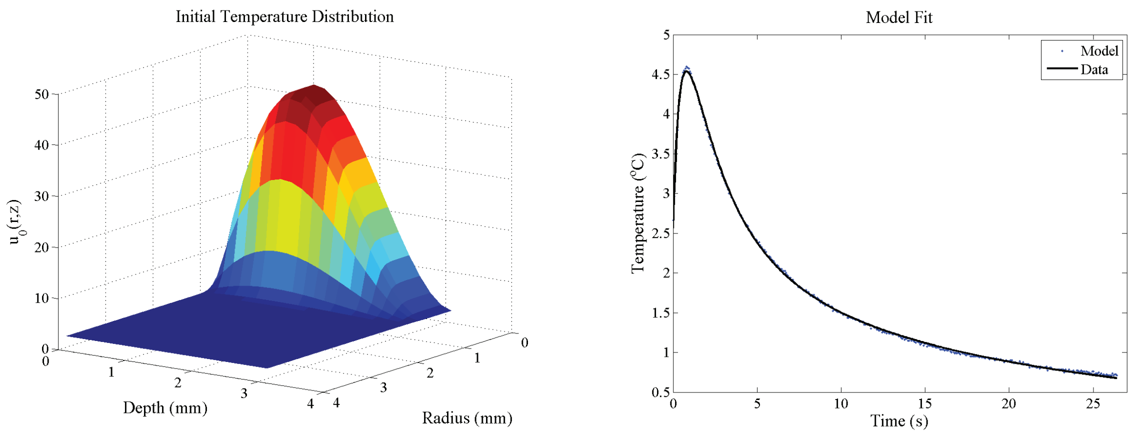

(a) (b)

FIGURE 5. (a) Estimated initial temperature distribution using (10) (b) Resulting fit

The initial condition (9) when used in data analysis yielded anomalous thermal diffusivity estimates. Splines were then used to estimate the z-dependence of the initial temperature distribution. The initial condition was given by

$$u_0(r,z) = \frac{T_L f(z)}{\left(1 + e^{15(r-r_0)}\right)} + T_R, \tag{10}$$

where $f(z)$ is a cubic polynomial with nodes at $z = 0$ and $z = L$. The value at $z = L$ was fixed to be zero, the temperature at $z = 0$, and derivatives with respect to z at the nodes were estimated. The estimated initial temperature distribution and model fit are depicted in Figures 5(a) and (b), respectively. The results were similar to fit using the logistic dependence in z. The similarity in the estimated curves is not surprising. Estimating the initial temperature distribution in the heat equation is ill-posed in the sense that many different initial temperature profiles will yield the same or similar results. This can be seen by comparing the temperature profiles in Figures 4 and 5(a) and then comparing the resultant models in Figures 4 and 5(b). The estimated thermal diffusivity was also an order of magnitude lower than the handbook value. When another node was added to the spline, the results were similar.

Many other initial temperature distributions and boundary conditions were used. A trigonometric source was used, with a poor fit and thermal diffusivity within the same range as the other thermal diffusivity estimates. Initial temperature distributions that are not presented here were also used, including products of trigonometric and exponential and products of splines and exponentials. These fits were also poor with thermal diffusivity estimates that were an order of magnitude lower than the handbook value of the thermal diffusivity.

Conclusions and Future Work

The work here illustrates the difficulties with data analysis. The results were anomalous. The observed thermal diffusivity estimates were not within the range of the handbook values though this behavior is consistent with these experiments carried out on other Ti-6Al-4V samples with different geometries. The sample will be interrogated with other methods to determine its thermal diffusivity. The behavior of the horn and possible other physics will also be investigated. Further work, once the estimation for a single location is carried out, will be done to incorporate all of the observed locations.

ACKNOWLEDGMENTS

The authors would like to thank Josiah Dierken, Shamachary Sathish and Matt Cherry for their discussions and insights. Some of this work was carried out under USAF contract FA8650-14-D-5224-0001.

REFERENCES

1 S. Sathish, J. T. Welter, K. V. Jata, N. Schehl, and T. Boehnlein, Review of Scientific Instruments **83**, p. 095103 (2012).
2 S. Sathish, J. T. Welter, N. Schehl, and K. V. Jata, "Non-contact acousto-thermal signatures in as received and fatigue damaged Ti-6Al-4V," in *Review of Progress in Quantitative Nondestructive Evaluation*, eds. D. E. Chimenti, L. Bond, and D. Thompson, (American Institute of Physics 1581 Mellville, NY) 33, 697-702 (2014).
3 H. Banks and A. K. Criner, Inverse Problems **28**, p. 065021 (2012).
4 H. T. Banks and B. Fitzpatrick, Journal of Mathematical Biology **28**, 501–527 (1990).
5 H. T. Banks, S. Hu, Z. R. Kenz, C. Kruse, S. Shaw, J. R. Whiteman, M. P. Brewin, S. E. Greenwald, and M. J. Birch, Journal of Inverse and Ill-Posed Problems **21**, 25–57 (2013).
6 K. P. Burnham and D. R. Anderson, *Model Selection and Inference: A Practical Information-Theoretical Approach* (Springer-Verlag, 1998).
7 W. Parker, R. Jenkins, C. Butler, and G. Abbott, Journal of Applied Physics **32**, 1679–1684 (1961).
8 T. Eagar and A. Mazzeo, in *ASM Handbook*, Vol. 6A (ASM International, 2011).
9 P. Ŝolín, *Partial differential equations and the finite element method*, Vol. 73 (John Wiley & Sons, 2005).